*electronics*

MDPI

*Article*

# Research on the Impact of the Interaction Between Renewable Energy and Loads on the Voltage Characteristics of Receiving-End Grids and Control Strategies

**Yi Wang [1], Zeyuan An [1] and Long Peng [2,*]**

[1] School of Electrical Engineering, Northeast Electric Power University, Jilin 132012, China; 2202200165@neepu.edu.cn (Y.W.); 2202200140@neepu.edu.cn (Z.A.)
[2] China Electric Power Research Institute, Haidian District, Beijing 100192, China
* Correspondence: penglong@epri.sgcc.com.cn

**Abstract:** As large-scale renewable energy sources are integrated into the receiving-end grid, their interaction with load demands careful examination. This paper begins by analyzing the characteristics of active and reactive power fluctuations in renewable energy sources during low-voltage ride-through (LVRT). For a typical single-machine system connected to the grid, the mathematical relationship between the output power of renewable energy sources and the voltage at the point of common coupling is derived, determining the operating range without entering the LVRT state. By incorporating load models into the mathematical analysis, it is shown that the correlation between active power and voltage varies according to the load proportion. This leads to the identification of two types of "repeated LVRT" mechanisms dominated by either active or reactive power. Furthermore, considering the dynamic load model, motor slip is shown to affect the stable operating range of renewable energy sources, contributing to LVRT phenomena. Finally, from the perspective of the relationship between the operating point of renewable energy and the LVRT threshold curve, optimization strategies are proposed to address several types of new voltage stability issues caused by the interaction of various loads. The feasibility of these voltage phenomena and control strategies is validated using a simulated model.

**Keywords:** renewable energy sources; low-voltage ride-through; load characteristics; induction motors; control measures



**Citation:** Wang, Y.; An, Z.; Peng, L. Research on the Impact of the Interaction Between Renewable Energy and Loads on the Voltage Characteristics of Receiving-End Grids and Control Strategies. *Electronics* **2024**, *13*, 4923. https://doi.org/10.3390/electronics13244923

Academic Editor: Ahmed Abu-Siada

Received: 17 October 2024
Revised: 4 December 2024
Accepted: 10 December 2024
Published: 13 December 2024



## 1. Introduction

As fossil fuel reserves continue to deplete and environmental concerns intensify, renewable energy sources have emerged as a viable solution to replace traditional coal-fired power plants. Renewable energy is regarded as the inevitable trend for future global power development [1]. In 2023, global renewable energy added 50% more capacity compared to 2022, with the rate of installation growth faster than at any point in the past 30 years. Against this backdrop, the replacement of conventional power sources by a high proportion of renewable energy is leading to a "hollowing out" trend in receiving-end power grids. Unlike traditional synchronous generators, the dynamic characteristics of renewable energy units are primarily determined by control strategies. The large-scale integration of renewable energy alters the dynamic behavior of receiving-end grids [2], leading to various new voltage stability issues [3,4].

Stability problems triggered by system faults include static and transient stability issues [4], which become more pronounced with the integration of renewable energy. Currently, scholars both domestically and internationally have made some research progress in addressing stability issues arising from renewable energy integration. Refs. [5–7] studied static voltage stability problems in systems with renewable energy integration and proposed related indicators, such as short-circuit ratios and impedance margins. Refs. [8,9] examined

the transient characteristics of low-voltage ride-through (LVRT) under large disturbances, explaining how it can cause overvoltage and voltage instability. Increasing numbers of renewable energy sources connected to the grid via power electronic converters reduce system damping [10], adversely affecting the oscillatory stability of power systems [11–13].

In considering the interaction between renewable energy sources and loads upon their integration into the receiving-end grid, ref. [14] analyzed the impact of load model variations on system voltage stability. Meanwhile, ref. [15] employed an efficient dynamic analysis method to investigate the influence of induction motor loads on voltage stability. Additionally, the interaction between renewable energy sources and induction motors can also lead to different characteristics [16,17].

Existing studies have extensively explored control strategies for renewable energy integration, focusing on the coordination of active and reactive power, system stability control, and fault recovery. For example, references [18–21] propose a series of methods for optimizing power scheduling, power smoothing, and energy management with storage devices to improve the stability of renewable energy systems connected to the grid. These studies cover various renewable energy sources, such as photovoltaic, wave energy, and hybrid microgrids, and emphasize the importance of flexible energy management strategies in reducing power fluctuations and enhancing voltage stability. Furthermore, references [22,23] investigate the coordination of active and reactive power dispatch and dynamic control in wind power systems under high renewable energy penetration. These studies present coordinated control and multi-mode scheduling methods that effectively enhance the grid's ability to handle fluctuations and faults. Regarding smart grid operation and fault stability, references [24,25] examine emergency response strategies, such as frequency and voltage regulation using supercapacitors, to improve the grid's fault recovery and disturbance resistance. Although these studies offer several solutions for power scheduling and grid stability, most focus on static control strategies and fault response, with limited consideration of the dynamic interactions between renewable energy sources and loads, as well as their impact on LVRT phenomena.

This paper systematically analyzes the relationship between the LVRT threshold and the operating point of the receiving-end grid during the integration of renewable energy. It reveals a new voltage instability phenomenon caused by the interaction between renewable energy and loads. The study finds two new types of low-voltage ride-through phenomena—"repeated low-voltage ride-through" and "sustained low-voltage ride-through"—triggered by control-state transitions. These phenomena exhibit different voltage oscillation characteristics under the dominance of active and reactive power. The voltage oscillations dominated by active power have smaller amplitudes and lower frequencies, while those dominated by reactive power show larger amplitudes and higher frequencies. This finding provides a new perspective for studying voltage stability during the integration of renewable energy. In addition, this paper further investigates how the slip of motor loads affects the power–voltage relationship in renewable energy systems. Specifically, during fault events, an increase in load slip may reduce the region of safe and stable operation for renewable energy systems, thus triggering low-voltage ride-through phenomena.

In response to these new voltage instability phenomena, this paper proposes corresponding control strategies, particularly by lowering the low-voltage ride-through threshold to effectively mitigate the "repeated low-voltage ride-through" and "sustained low-voltage ride-through" caused by the interaction between renewable energy and loads. Simulation results validate the effectiveness of these control strategies, providing theoretical support and practical guidance for voltage stability research after renewable energy integration.

## 2. PQ Safe and Stable Operation Range Considering Renewable Energy Ride-Through Control

This section begins by analyzing the LVRT characteristics of renewable energy systems. By combining power flow and voltage constraints, the safe operating region of power and voltage for renewable energy systems is determined.

### *2.1. LVRT Characteristics of Renewable Energy*

When significant disturbances, such as short circuits, cause voltage drops in the grid, most renewable energy systems employ LVRT control mechanisms [26–28] (This paper studies the photovoltaic system as an example of a renewable energy system). The system defines threshold values, $U_{sL}$ and $U_{sH}$, for entering and exiting LVRT. When the voltage at the point of common coupling ($U_{PCC}$) drops below the entry threshold $U_{sL}$, the control strategy shifts from normal operation to LVRT fault-period control. When $U_{PCC}$ exceeds the exit threshold $U_{sH}$, the control strategy transitions from LVRT fault-period control to post-fault power ramp-up control, eventually returning to normal operation.

If the renewable energy unit enters the LVRT control state, its active power will rapidly decrease due to the voltage drop at the point of common coupling and gradually recover once the LVRT period ends. During LVRT, reactive power will increase to support voltage at the point of common coupling and will cease rising and revert to normal control strategies once the LVRT period ends.

The specific active power control measures are illustrated in Figure 1. During LVRT, the active current can be flexibly controlled to regulate the active power output of the renewable energy unit. In the post-LVRT recovery process, three common methods are used to restore active power to normal levels: immediate recovery, recovery with a specified slope, and parabolic recovery. An initial power ramp-up value can also be specified at the start of the recovery process.

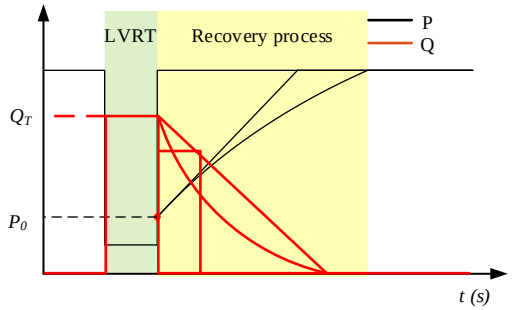


**Figure 1.** Power control during LVRT and recovery process.

The specific reactive power control measures are illustrated in Figure 1. During LVRT, the reactive current injected by the renewable energy system into the grid should meet the following requirements: from the moment the voltage at the point of connection drops, the dynamic reactive current response time should not exceed 30 ms; from the start of the reactive current response until the voltage recovers to the exit threshold of the low-voltage ride-through, the reactive current $I_T$ injected by the renewable energy system into the grid should track the voltage changes at the point of connection in real time and should meet the following conditions:

$$\begin{cases} I_T \geq 1.5 \times (0.9 - U_T) I_N \ (0.2 \leq U_T \leq 0.9) \\ I_T \geq 1.5 \times I_N \ (U_T < 0.2) \\ I_T = 0 \ (U_T > 0.9) \end{cases} \quad (1)$$

where $U_T$ is the per-unit voltage at the renewable energy point of common coupling and $I_T$ is the rated current of the renewable energy system.

In the post-LVRT recovery process, four common methods are employed to restore reactive power to normal levels: immediate recovery, recovery with a specified slope, parabolic recovery, and maintaining a constant value for a specified period before recovery.

### *2.2. P-Q-V Characteristic Curve of Renewable Energy*

After renewable energy is integrated into the power grid, its output power plays a key role in the stability of both the grid and the renewable energy system itself. Based on the single-machine infinite bus equivalent system shown in Figure 2, the impact of the power output of renewable energy on the voltage at the point of common coupling is analyzed.

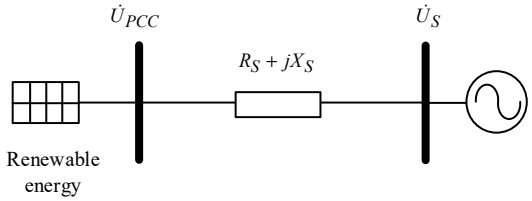


**Figure 2.** Single renewable energy generator to infinite bus system.

The renewable energy side is equivalent to a power source, its output active power is $P_{\mathrm{w}}$, and its reactive power is $Q_{\mathrm{w}}$; then, there is a relationship [26]:

$$P_W + jQ_W = U_{PCC}\angle\theta\left(\frac{U_{PCC}\angle\theta - U_S\angle 0}{R_S + jX_S}\right)^* \tag{2}$$

where $U_{\mathrm{PCC}}$ is the voltage of the renewable energy point of common coupling, $\theta$ is the phase angle of parallel nodes, $U_{\mathrm{S}}$ is the infinite side voltage, and $R_{\mathrm{S}}$ + j$X_{\mathrm{S}}$ is the connection impedance.

The relationship between the sent power of new energy and the voltage of the connecting point is obtained as follows:

$$P_W = \frac{U_{PCC}^2}{R_S + jX_S}\cos\theta_z - \frac{U_{PCC}U_S}{R_S + jX_S}\cos(\theta_z + \theta) \tag{3}$$

$$Q_W = \frac{U_{PCC}^2}{R_S + jX_S}\sin\theta_z - \frac{U_{PCC}U_S}{R_S + jX_S}\sin(\theta_z + \theta) \tag{4}$$

where $\theta_z$ is the impedance angle.

Subtract $\theta$ from the above formula to obtain the following:

$$(P_W - \frac{U_{PCC}^2}{R_S + jX_S}\cos\theta_z)^2 + (Q_W - \frac{U_{PCC}^2}{R_S + jX_S}\sin\theta_z)^2 = (\frac{U_{PCC}U_S}{R_S + jX_S})^2 \tag{5}$$

Solve the voltage of the renewable energy junction:

$$\begin{aligned} U_{PCC} &= F(P_W, Q_W, X_S, R_S, U_S) \\ &= \sqrt{\frac{U_S^2}{2} + Q_W X_S + P_W R_S + \sqrt{\frac{U_S^4}{4} + (P_W R_S + Q_W X_S)U_S^2 + 2P_W R_S Q_W X_S + P_W^2 R_S^2 + Q_W^2 X_S^2 - (R_S^2 + X_S^2)(P_W^2 + Q_W^2)}} \end{aligned} \tag{6}$$

According to Equation (6) and the LVRT threshold, the projection of the LVRT threshold of the renewable energy unit onto the PQ plane, when connected to an infinite bus, is shown in Figure 3.

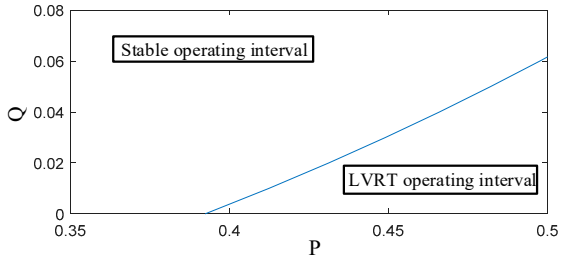


**Figure 3.** Projection of the boundary line on the PQ plane.

When the output power of renewable energy is above the projection dividing line, the renewable energy is a stable-operation control strategy. When the output power of the renewable energy is under the projection dividing line, the renewable energy is an LVRT control strategy, and the PQ interval of the safe and stable operation of the renewable energy can be obtained.

## 3. Recurrent LVRT Phenomenon Dominated by Active and Reactive Power

The voltage interaction between renewable energy and the grid depends on the power–voltage characteristics of both the system side and the renewable energy side. Considering the integration of different load proportions, the power–voltage characteristics of the system side vary. This section first analyzes the impact of load proportions on the PQV characteristics of the system and then derives the recurrent LVRT phenomena dominated by active and reactive power.

### *3.1. Impact of Load Ratio on the PQV Characteristic Curve*

The size of the load directly affects the power balance, grid operating conditions, and voltage-regulation capabilities of the system. Therefore, different load proportions have a significant impact on the relationship between the point of common coupling voltage and the output power of renewable energy.

A single-machine renewable energy system is constructed as shown in Figure 4. The renewable energy system is connected to an infinite bus grid via a double-circuit line. Under normal circumstances, the renewable energy system is connected to the grid through an inverter. In this study, we mainly focus on the power output of the renewable energy system. Therefore, to simplify the discussion, the inverter connection is not shown in detail in the diagram. The system parameters are shown in Table 1.

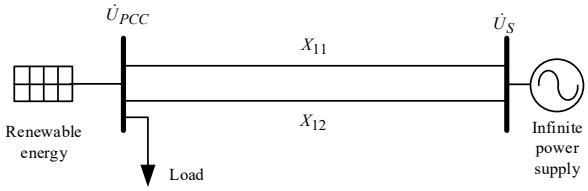


**Figure 4.** Renewable energy standalone system.

**Table 1.** Initial operating parameters of standalone renewable energy system.

| $X_{11}$ (p.u.) | $X_{12}$ (p.u.) | $P$ (MW) | $P_L$ (MW) |
|---|---|---|---|
| 0.3 | 0.3 | 1000 | 2000 |

Based on the parameters in Table 1, a three-phase ground fault occurs on the double-circuit line at the renewable energy side at 0.2 s, and Line 2 is disconnected at 0.4 s. The point of common coupling voltage and the active power output for renewable energy under load sizes of 2000 MW and 100 MW are shown in Figures 5a and 5b, respectively.

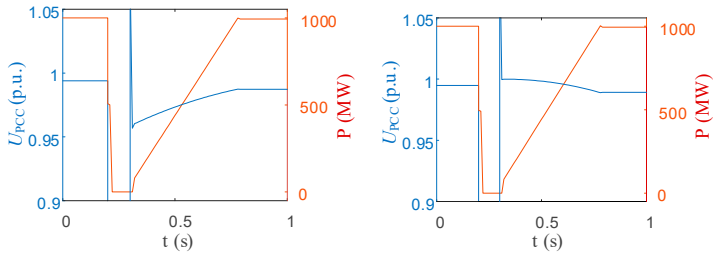


(a) under high load conditions (b) under low load conditions

**Figure 5.** Relationship between active power and voltage for different load ratios in renewable energy systems.

As shown in Figure 5a, during the fault, the renewable energy system enters the low-voltage ride-through control strategy, and the active power drops to zero. After the fault disconnection, the voltage recovers above the LVRT threshold, and the active power recovers along the slope. As active power increases along the recovery slope, the point of common coupling voltage increases accordingly. When the load is reduced to 100 MW, as shown in Figure 5b, the smaller load proportion leads to a different behavior. After the fault disconnection, the point of common coupling voltage decreases as the active power increases.

Simulations show that the correlation between the point of common coupling voltage and the active power output of renewable energy depends on the load proportion, affecting the PQV characteristic curve of renewable energy.

### *3.2. Recurrent LVRT Phenomenon Dominated by Active Power*

The control-strategy switching behavior in renewable energy systems leads to novel voltage instability phenomena. When renewable energy systems switch between the normal control mode and the low-voltage ride-through control mode, different operating equilibrium points in the power system can cause abnormal voltage behavior. Particularly when the operating point repeatedly switches between different control strategies, a recurrent LVRT phenomenon can occur, causing repeated fluctuations in the point of common coupling voltage and affecting the safe and stable operation of the power system.

In the single-machine renewable energy system (Figure 4), a 100 MW load is connected near the renewable energy side. From Equation (6), the relationship between the renewable energy output power and the point of common coupling voltage is shown in Figure 6.

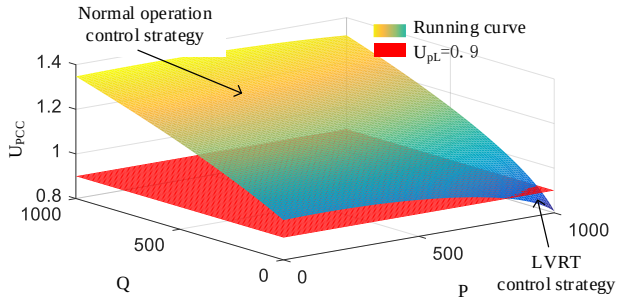


**Figure 6.** Relationship between renewable energy output power and grid voltage under low-load conditions.

As shown in the figure, when the load proportion is small, the larger the active power output of renewable energy, the lower the point of common coupling voltage. On the other hand, the larger the reactive power output of renewable energy, the higher the point of common coupling voltage.

Projecting the surface onto the PQ plane, the contour lines represent the point of common coupling voltage, as shown in Figure 7.

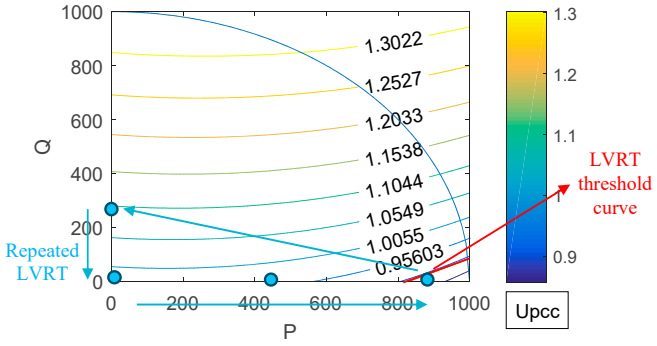


**Figure 7.** Movement of operating point during repeated LVRT under low-load conditions.

When the threshold curve falls within the active power recovery process at a slope, the operating point will repeatedly switch between the normal control strategy range and the low-voltage ride-through control strategy range, resulting in a recurrent LVRT phenomenon. In this case, the phenomenon occurs during the active power recovery process, starting from the stable operating range and entering the LVRT range, then exiting the LVRT range and returning to the stable range. This cycle leads to the recurrent LVRT phenomenon, with the voltage fluctuating slowly due to the gradual recovery of active power along the slope.

In the single-machine renewable energy system shown in Figure 4, under the initial conditions in Table 1, the impedance of Line 1 is set to 0.6 p.u. and the impedance of Line 2 is set to 0.6 p.u. The load is adjusted to 100 MW. A fault is set where a three-phase ground fault occurs on the double-circuit line at the renewable energy side at 0.2 s, and Line 2 of the double-circuit line is disconnected at 0.3 s. The point of common coupling voltage and the active/reactive power output of renewable energy are shown in Figure 8.

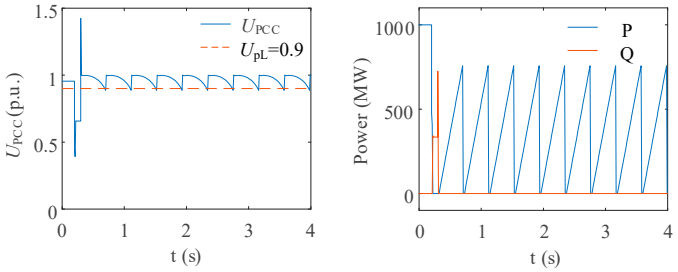


(a) the voltage at the point of interconnection

(b) power output of new energy sources

**Figure 8.** Relevant parameters for repeated LVRT under low-load conditions.

In Figure 8a, after the fault disconnection, the point of common coupling voltage oscillates repeatedly around the LVRT threshold with a slow oscillation speed. As shown in Figure 8b, during the fault, the active power of renewable energy drops to zero, and after the fault disconnection, active power recovers along the slope. This recovery process causes a voltage drop, resulting in a recurrent LVRT phenomenon dominated by active power, as described earlier.

### *3.3. Recurrent LVRT Phenomenon Dominated by Reactive Power*

In the single-machine renewable energy system with a 2000 MW load connected near the renewable energy side, as shown in Figure 9, the relationship between the renewable energy output power and the point of common coupling voltage is plotted.

As shown in the figure, when the load proportion is large, the larger the active power output of renewable energy, the higher the point of common coupling voltage. Similarly, the larger the reactive power output, the higher the point of common coupling voltage.

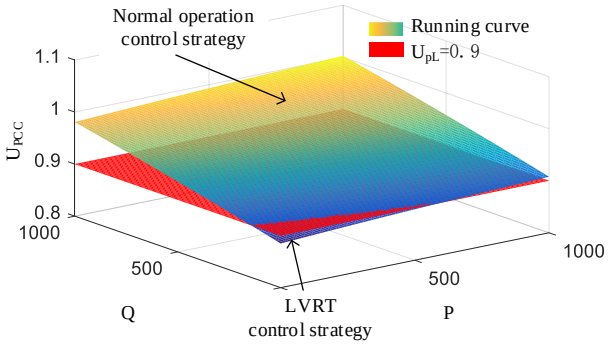


**Figure 9.** Relationship between renewable energy output power and grid voltage under high-load conditions.

Projecting the surface onto the PQ plane, the contour lines represent the point of common coupling voltage, as shown in Figure 10.

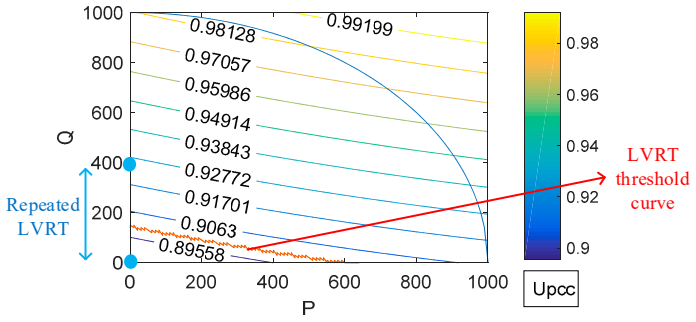


**Figure 10.** Movement of operating point during repeated LVRT under high-load conditions.

When the threshold curve falls between the operational point of the LVRT control strategy and the initial point of the active power recovery slope, the operating point will repeatedly switch between the normal control strategy range and the LVRT control strategy range, resulting in a recurrent LVRT phenomenon.

When the load proportion is big, the recurrent LVRT phenomenon occurs immediately after the fault is cleared, dominated by the reactive power output of the renewable energy unit during LVRT. The system exits the LVRT range and enters the stable operating range, then re-enters the LVRT range, leading to repeated LVRT. Due to the rapid switching between two operational points, the voltage oscillation rate is fast.

In the single-machine renewable energy system shown in Figure 4, under the initial conditions in Table 1, the impedance of Line 1 is set to 0.1 p.u. and the impedance of Line 2 is set to 0.4 p.u., with other parameters unchanged. When the load is set to 2000 MW and the LVRT threshold is set to 0.9 p.u., a fault is set where a three-phase ground fault occurs on the double-circuit line at 0.2 s, and Line 2 is disconnected at 0.3 s. The point of common coupling voltage and the active/reactive power output of renewable energy are shown in Figure 11.

As shown in Figure 11a, after the fault disconnection, the point of common coupling voltage oscillates repeatedly around the LVRT threshold, with a rapid oscillation speed. According to Figure 11b, after the fault disconnection, the point of common coupling voltage recovers above the threshold and the reactive power output drops to zero, causing the voltage to fall below the threshold again. This triggers reactive power output, raising the voltage again and resulting in repeated voltage fluctuations, which causes a recurrent LVRT phenomenon dominated by reactive power.

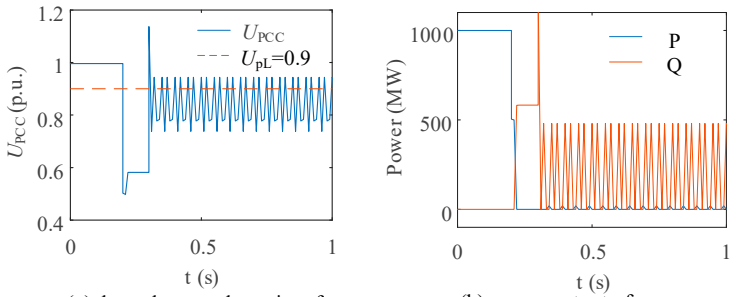


(a) the voltage at the point of interconnection

(b) power output of new energy sources

**Figure 11.** Relevant parameters for repeated LVRT under high-load conditions.

## 4. Impact of Motor Characteristics on the Safe and Stable Operation Range

In the aforementioned research, the focus is primarily on voltage stability issues caused by the size of the load when the load model is considered as constant impedance. However, within the load of the receiving grid, motor loads are a significant component, and the dynamic characteristics of motors have a more pronounced impact on voltage. Therefore, when renewable energy is integrated into the receiving grid, the interaction between motors and renewable energy is worthy of further study. This section further analyzes the impact of motors on the power–voltage characteristics of grid-connected renewable energy, investigates how the dynamic characteristics of motors affect the LVRT control state of renewable energy, and proposes control strategies to ensure the stability of renewable energy operations.

### *4.1. Power–Voltage Characteristics of Motors in the System*

Dynamic changes in load are mainly caused by variations in the slip of the motor, which is a key factor affecting the voltage stability and safety of the power system. The static equivalent circuit of an induction motor is shown in Figure 12, where $R_S$ represents the stator resistance, $X_s$ is the stator reactance, $X_M$ is the magnetizing reactance, $R_r$ is the rotor resistance, and $X_r$ is the rotor reactance.

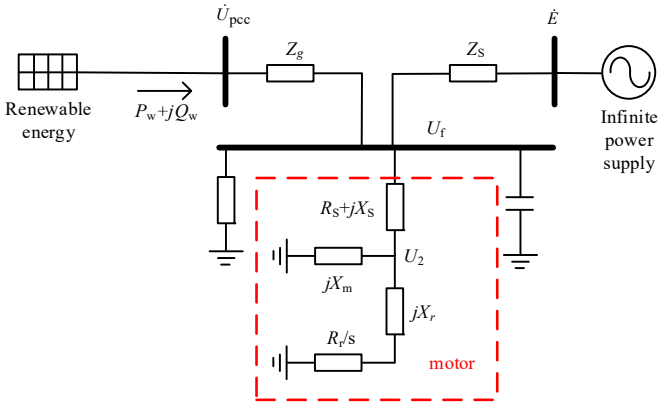


**Figure 12.** System topology diagram with the addition of the motor.

The equivalent impedance of motor loads is not a constant value; it varies with the slip s, which is determined by the operating state of the motor. As the slip s increases, the equivalent impedance of the motor decreases. A load is added to the original renewable energy system connected to the infinite bus, as shown in Figure 12. The load model includes constant impedance loads, motor loads, and reactive power compensation. The constant impedance load and motor load are proportionally distributed, with the reactive power compensation responsible for compensating the reactive power absorbed by the motor load.

Using Thevenin's theorem, the rest of the system outside the renewable energy source is equivalent to a voltage source ($U_{11}$) and an impedance ($Z_{11}$), as shown in Figure 13.

$$U_{11} = \frac{E}{Z_s + Z_f} \times Z_f \tag{7}$$

$$Z_{11} = \frac{1}{\frac{1}{Z_s} + \frac{1}{Z_f}} + Z_g = R_{11} + jX_{11} \tag{8}$$

where $Z_S$ is the infinite bus impedance, $Z_f$ is the renewable energy access impedance, and $Z_g$ is the equivalent load impedance.

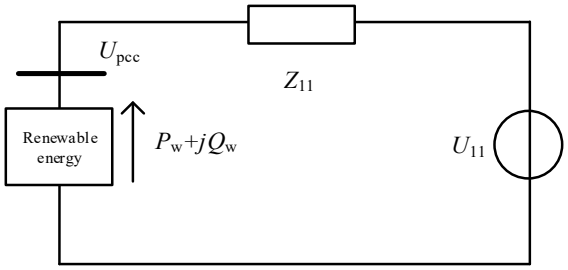


**Figure 13.** System topology diagram after the implementation of the Thevenin equivalent circuit.

Substituting the parameters after Thevenin's equivalent into Equation (6), the relationship between the renewable energy output power and the grid voltage after incorporating the motor load model can be derived, as shown in Equation (9).

$$\begin{aligned} U_{PCC} &= F(P_W, Q_W, X_{11}, R_{11}, U_{11}) \\ &= \sqrt{\begin{array}{l} \frac{U_{11}^2}{2} + Q_W X_{11} + P_W R_{11} \\ + \sqrt{\begin{array}{l} \frac{U_{11}^4}{4} + (P_W R_{11} + Q_W X_{11}) U_{11}^2 + 2P_W R_{11} Q_W X_{11} \\ + P_W^2 R_{11}^2 + Q_W^2 X_{11}^2 - (R_{11}^2 + X_{11}^2)(P_W^2 + Q_W^2) \end{array}} \end{array}} \end{aligned} \tag{9}$$

In the system illustrated in Figure 13, let the renewable energy access impedance $Z_f$ = j0.01 and the infinite bus impedance $Z_S$ = j0.1 (the electrical distance between the receiving-end renewable energy and the load is much smaller than the distance between the infinite bus and the load). The total load is 2 p.u. (based on a 1000 MVA system), with 50% of the load being motors. The motor parameters are listed in Table 2 (based on motor capacity).

**Table 2.** Typical parameters of the motor.

| $R_S$ (p.u.) | $X_s$ (p.u.) | $X_M$ (p.u.) | $R_R$ (p.u.) | $X_R$ (p.u.) |
|---|---|---|---|---|
| 0.02 | 0.18 | 3.499 | 0.02 | 0.12 |

By normalizing all parameters to the same base value and substituting them into Equation (9), the projection of the intersection between the relationship curve and the LVRT threshold plane on the PQ plane is obtained, as shown in Figure 14. In this figure, the slips of the induction motor is a variable that fluctuates as the system experiences disturbances.

As shown in Figure 14, the projection curve of the LVRT threshold under different slips (blue line) and the boundary of the safe and stable operating region of the renewable energy (red line) constrain the operating region. As the slip increases, the LVRT threshold curve moves upward, reducing the safe operating region.

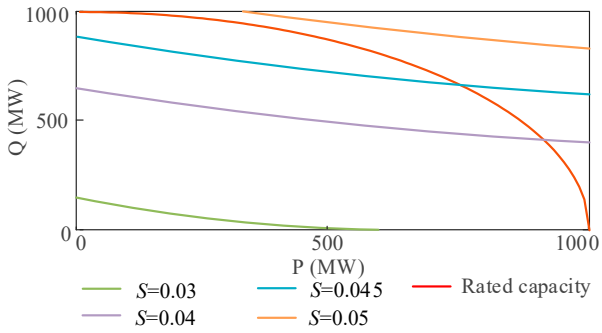


**Figure 14.** Stable operating range of renewable energy system after the addition of the motor.

*4.2. LVRT Phenomenon Dominated by Motor Slip*

As described in Section 3.1, due to the interaction between the renewable energy output power and motor slip, large disturbances in the system cause variations in motor slip, which in turn affect the safe and stable operating region of the renewable energy system. This section will verify this effect.

In the single-machine renewable energy system shown in Figure 4, under the initial conditions of Table 1, the impedance of Line 2 is set to 0.2 p.u. and the load model is changed to 50% induction motor + 50% constant impedance load, while other parameters remain unchanged.

At 0.2 s, a three-phase ground fault occurs on Line 2 of the double-circuit line, and at 0.5 s the faulted line is disconnected. The system voltage at the renewable energy point of common coupling is recorded for two load models: 50% induction motor + 50% constant impedance and 100% constant impedance, as shown in Figure 15.

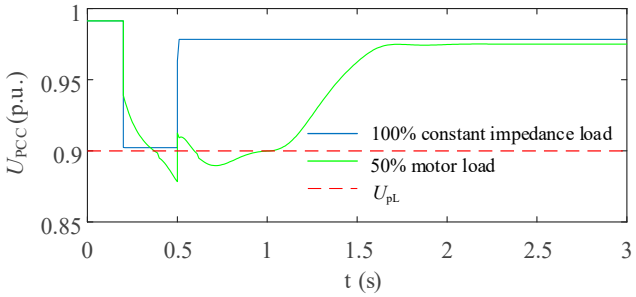


**Figure 15.** Voltage at the point of common coupling for different load models with renewable energy integration.

As can be seen from the figure, when the load model is 100% constant impedance, the voltage at the renewable energy point of common coupling remains stable after dropping to a certain value during the fault. However, for the 50% induction motor load model, the voltage continues to decrease during the fault, as the slip of the induction motor changes, affecting the voltage.

As shown in Figure 16, during the fault (represented by the yellow shaded area), the slip of the induction motor increases as the system experiences the three-phase short-circuit fault. This leads to a gradual reduction in the safe and stable operating region of the renewable energy system, causing the grid voltage at the point of common coupling to drop below the LVRT threshold, triggering the LVRT control strategy.

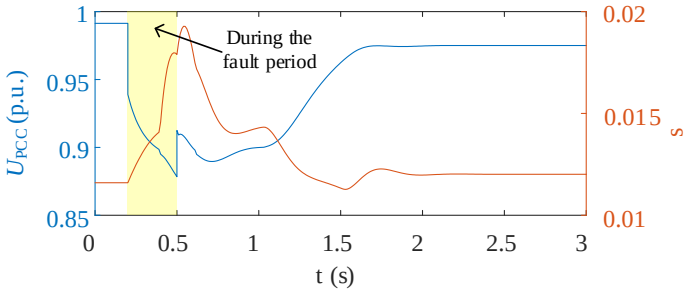


**Figure 16.** Relationship between slip ratio of induction motor and renewable energy voltage.

## 5. Optimization Strategies for New Types of Voltage Instability and Grid Connection Requirements

This section builds upon the analysis of repeated LVRT phenomena dominated by active and reactive power and the impact of motor characteristics on the safe and stable operating region of renewable energy grid integration. It further proposes optimizing control parameters for renewable energy integration to improve its safety and stability.

### *5.1. Optimization Strategy Requirements for the Recurrent LVRT Phenomenon*

During large disturbances, the dynamic LVRT process causes the operating point of grid-connected renewable energy units to fluctuate repeatedly. Therefore, optimizing control parameters during the LVRT recovery process to prevent the operating point from oscillating around the threshold curve is key to addressing the "repeated LVRT" phenomenon, which is also a critical requirement for renewable energy grid integration.

As shown in Figure 17a, the operating state of renewable energy during the LVRT process is illustrated, with the blue shading representing the changes in active and reactive power: After the renewable energy unit enters LVRT, it generates reactive power, leaving a trajectory on the Q-axis; when exiting LVRT, reactive power drops to zero, and active power begins recovering from zero along a slope, leaving a trajectory on the P-axis. The two black curves represent the LVRT threshold under high- and low-load conditions. In the case of Figure 17a, both threshold curves intersect with the operating trajectory, causing the unit to switch between normal control and LVRT control, leading to the "repeated LVRT" phenomenon. To prevent these voltage oscillations, a control strategy is needed to adjust system parameters so that the threshold curve does not intersect with the operating trajectory. The control strategies are as follows:

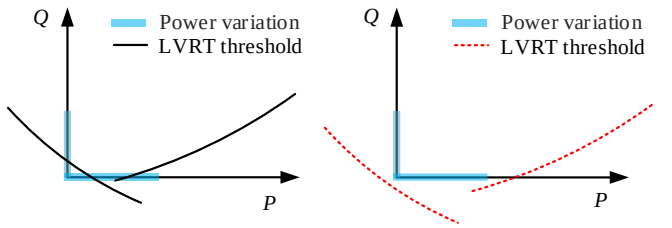


**Figure 17.** Diagram of renewable energy operating regions.

Lower the LVRT threshold: As shown in Figure 17b, shifting the LVRT threshold curve downward ensures that the entire operating process of the renewable energy unit remains within the safe and stable region.

To verify these strategies, a single-machine renewable energy system was simulated using the PSDEdit 2.9 simulation software, as shown in Figure 4. The proposed strategies were applied to address the "repeated LVRT" phenomenon under both high- and low-load conditions. Plan 1, which lowers the LVRT threshold voltage $U_{pL}$, was tested by reducing the LVRT threshold from 0.9 to 0.7 under high-load conditions (2000 MW) and from 0.9 to

0.8 under low-load conditions (100 MW). The transient response comparisons are shown in Figure 18a,b. According to the simulation results, lowering the LVRT threshold effectively prevents the "repeated LVRT" phenomenon, regardless of load size.

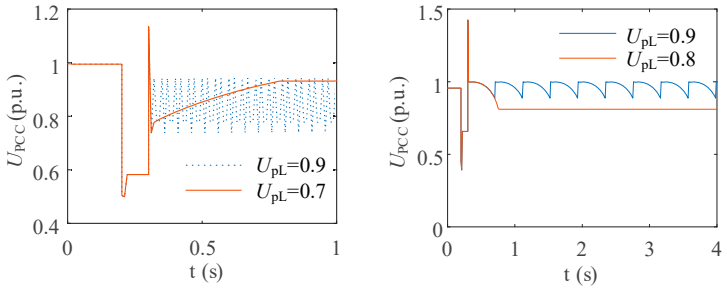


(a) the power receiving end (b) the power sending end

**Figure 18.** Comparison chart of voltage for Optimization Plan 1.

*5.2. Optimization Strategy Requirements for the LVRT Phenomenon Caused by Motor Slip*

The operating diagram of the renewable energy system is shown in Figure 19, where the operating point is located on the active power (P) axis, indicating that the unit is currently operating normally, generating active power. As the motor slip increases, the LVRT threshold curve gradually moves upward. When the curve crosses the operating point, the unit enters the LVRT operating state.

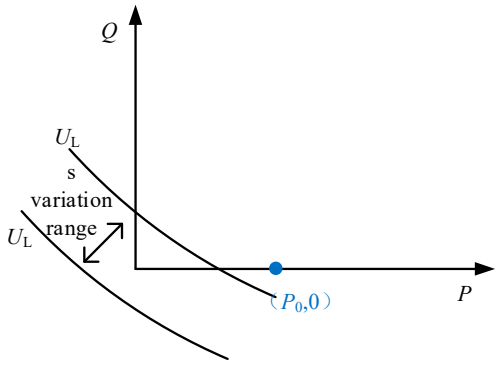


**Figure 19.** Threshold curve motion chart.

To ensure that the renewable energy unit operates safely and stably after the motor load is connected, a control strategy is proposed: lowering the LVRT threshold. By reducing the LVRT threshold below the voltage corresponding to the motor's maximum slip, the operating point can remain within the safe and stable operating region at all times.

To address the LVRT phenomenon caused by motor slip, a simulation system was set up, as shown in Figure 4. Under the initial conditions listed in Table 1, the impedance of Line 2 was changed to 0.15 p.u. A fault was introduced at 0.2 s, causing a three-phase ground short circuit on the renewable energy side of the double-circuit line, followed by a disconnection of Line 2 at 0.3 s. By lowering the LVRT threshold below the voltage corresponding to the motor's maximum slip (0.6 p.u.), the system's transient response comparison is shown in Figure 20.

After lowering the threshold, the voltage corresponding to the motor's maximum slip remains above the LVRT threshold. During the fault-clearing process, the motor slip recovery stays entirely within the safe and stable operating region of the renewable energy unit. This results in a more stable voltage recovery at the renewable energy point of common coupling and allows the unit to resume its normal active power output more quickly, enhancing system stability.

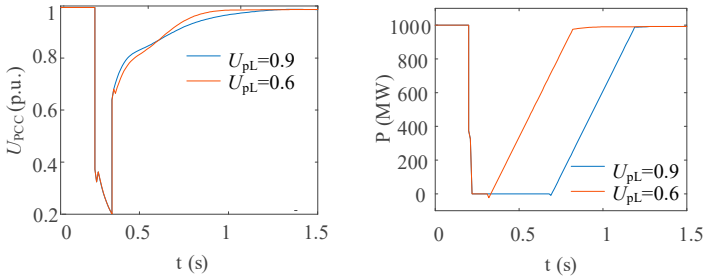


(a) the voltage at the point of interconnection (b) the active power

**Figure 20.** Comparison of electrical quantities related to renewable energy after lowering the threshold.

## 6. Case Studies

In response to the aforementioned repeated LVRT phenomenon, this study established a simulation model of the photovoltaic (PV) power generation system on a real-time simulation platform and constructed a PV inverter controller–real-time hardware-in-the-loop (HIL) test platform. A physical diagram of the platform is shown in Figure 21. The response data of the PV inverter were tested using this platform.


**Figure 21.** Platform physical map.

In the experiment, disturbances were applied to lower the voltage at the PV grid connection point to near the LVRT threshold, after which the voltage at the grid connection point began to fluctuate, as shown in Figure 22a. The changes in PV output power are shown in Figure 22b. The power fluctuations are caused by the transition in the LVRT control strategy; thus, these voltage fluctuations are categorized as repeated low-voltage ride-through phenomena. After implementing a control strategy to lower the threshold, the voltage fluctuations caused by repeated LVRT phenomena were significantly eliminated, as shown in Figure 22c.

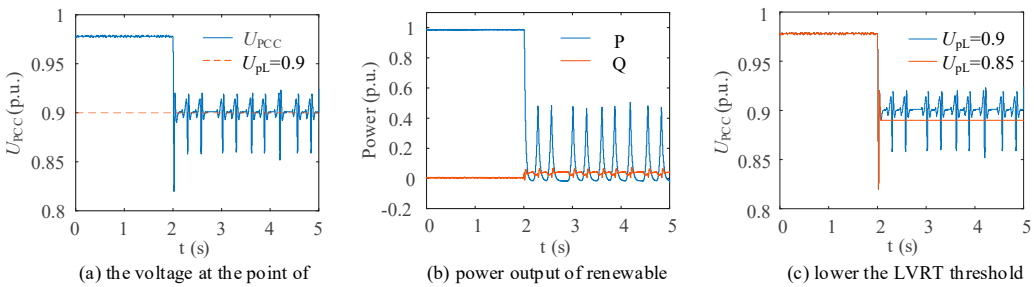


(a) the voltage at the point of interconnection (b) power output of renewable energy sources (c) lower the LVRT threshold

**Figure 22.** HIL experimental simulation diagram.

## 7. Conclusions

This paper analyzes the relationship between the LVRT threshold of renewable energy integration and its operating point in receiving-end power grids. It explains the mechanisms of new types of voltage instability caused by the interaction between renewable energy and load and proposes corresponding control strategies. The main conclusions are shown in Table 3:

(1) The interaction between the switching of renewable energy control states and the power–voltage characteristics of the grid leads to two new types of "repeated LVRT" phenomena dominated by active power and reactive power. Active power-dominated voltage oscillations have smaller amplitudes and lower frequencies, while reactive power-dominated oscillations have bigger amplitudes and higher frequencies.
(2) The slip of motor loads affects the power–voltage relationship at the renewable energy point of common coupling. During a fault, an increase in slip reduces the safe and stable operating region of renewable energy, leading to LVRT phenomena caused by slip.
(3) To address the "repeated LVRT" and "continuous LVRT" phenomena caused by the interaction between renewable energy LVRT characteristics and load, strategies such as lowering the LVRT threshold can effectively mitigate these new types of voltage instability.

**Table 3.** Main conclusions of this paper.

| Voltage Characteristics | Occurrence Time/Cause of Generation | Characteristics | Control Strategies |
|---|---|---|---|
| Recurrent LVRT phenomena | Under low-load conditions | Oscillations dominated by active power, with small amplitude and low frequency | Lowering the LVRT threshold |
| | Under high-load conditions | Oscillations dominated by reactive power, with large amplitude and high frequency | |
| LVRT phenomena caused by slip | The dynamic characteristics of motors | The LVRT phenomenon caused by changes in motor slip, which affect the voltage | |

Future work will focus on further developing control strategies for motors based on the optimization strategies for renewable energy systems, aiming to propose a comprehensive optimization scheme to ensure the overall safe and stable operation of power systems.

**Author Contributions:** Conceptualization, Y.W. and L.P.; methodology, Y.W.; software, Y.W.; validation, Y.W. and Z.A.; formal analysis, Y.W. and L.P.; investigation, Y.W; resources, L.P.; data curation, L.P.; writing—original draft preparation, Y.W.; writing—review and editing, Z.A.; visualization, Z.A.; supervision, Y.W. and Z.A; project administration, L.P.; funding acquisition, L.P. All authors have read and agreed to the published version of the manuscript.

**Funding:** This research received no external funding.

**Data Availability Statement:** The original contributions presented in the study are included in the article; further inquiries can be directed to the corresponding author.

**Conflicts of Interest:** Author Long Peng was employed by China Electric Power Research Institute. The remaining authors declare that the research was conducted in the absence of any commercial or financial relationships that could be construed as a potential conflict of interest.

## References

1. Taylor, J.A.; Dhople, S.V.; Callaway, D.S. Power systems without fuel. *Renew. Sustain. Energy Rev.* **2016**, *57*, 1322–1336. [CrossRef]
2. Kenyon, R.W.; Hoke, A.; Tan, J.; Hodge, B.-M. Grid-Following Inverters and Synchronous Condensers: A Grid-Forming Pair? In Proceedings of the 2020 Clemson University Power Systems Conference (PSC), Clemson, SC, USA, 10–13 March 2020; pp. 1–7.

3. Hao, W.; Chen, M.; Gan, D. Short-Term Voltage Stability Analysis and Enhancement Strategies for Power Systems with Photovoltaic Penetration. *IEEE Access* **2024**, *12*, 88728–88738. [CrossRef]
4. Li, X.; Li, Z.; Guan, L.; Zhu, L.; Liu, F. Review on Transient Voltage Stability of Power System. In Proceedings of the 2020 IEEE Sustainable Power and Energy Conference (iSPEC), Chengdu, China, 23–25 November 2020; pp. 940–947.
5. Wang, T.; Wang, S.; Ma, S.; Guo, J.; Zhou, X. An Extended Continuation Power Flow Method for Static Voltage Stability Assessment of Renewable Power Generation-Penetrated Power Systems. *IEEE Trans. Circuits Syst. II Express Briefs* **2024**, *71*, 892–896. [CrossRef]
6. Xin, H.; Liu, X.; Zheng, D.; Chen, D.; Zhou, Y. Marshall. Risk Assessment of Post-Fault Temporary Overvoltage Using Generalized Short-Circuit Ratio. *IEEE Trans. Power Syst.* **2024**, *39*, 1837–1849. [CrossRef]
7. Aik, D.L.H.; Andersson, G. Impact of renewable energy sources on steady-state stability of weak AC/DC systems. *CSEE J. Power Energy Syst.* **2017**, *3*, 419–430. [CrossRef]
8. Chen, S. Transient Stability Analysis and Improved Control Strategy for DC-Link Voltage of DFIG-Based WT During LVRT. *IEEE Trans. Energy Convers.* **2022**, *37*, 880–891. [CrossRef]
9. Liu, R.; Yao, J.; Wang, X.; Sun, P.; Pei, J.; Hu, J. Dynamic Stability Analysis and Improved LVRT Schemes of DFIG-Based Wind Turbines During a Symmetrical Fault in a Weak Grid. *IEEE Trans. Power Electron.* **2020**, *35*, 303–318. [CrossRef]
10. Prakash, A.; Moursi, M.S.E.; Parida, S.K.; Kumar, K.; El-Saadany, E.F. Damping of Inter-Area Oscillations with Frequency Regulation in Power Systems Considering High Penetration of Renewable Energy Sources. *IEEE Trans. Ind. Appl.* **2024**, *60*, 1665–1679. [CrossRef]
11. Meegahapola, L.G.; Bu, S.; Wadduwage, D.P.; Chung, C.Y.; Yu, X. Review on Oscillatory Stability in Power Grids with Renewable Energy Sources: Monitoring, Analysis, and Control Using Synchrophasor Technology. *IEEE Trans. Ind. Electron.* **2021**, *68*, 519–531. [CrossRef]
12. Tummala, A.S.L.V. A Robust Composite wide Area Control of a DFIG wind Energy System for Damping Inter-Area Oscillations. *Prot. Control Mod. Power Syst.* **2020**, *5*, 25. [CrossRef]
13. Wang, S.; Li, H.; Song, X.; Li, J.; Zhou, G.; Fang, J. Forced Oscillation Suppression Method of Renewable Energy High-Infiltration Power System Based on Kuramoto-like Model. In Proceedings of the 2021 IEEE 5th Conference on Energy Internet and Energy System Integration (EI2), Taiyuan, China, 22–24 October 2021; pp. 2918–2923.
14. Zhengqing, X.; Runzi, H.; Chunming, W.; Liying, Z.; Huankun, Z.; Yukai, L. Voltage Stability Analysis of AC/DC System Considering Static Load Characteristics. In Proceedings of the 2019 IEEE 3rd Conference on Energy Internet and Energy System Integration (EI2), Changsha, China, 8–10 November 2019; pp. 1284–1287.
15. Yao, R.; Sun, K.; Shi, D.; Zhang, X. Voltage Stability Analysis of Power Systems with Induction Motors Based on Holomorphic Embedding. *IEEE Trans. Power Syst.* **2019**, *34*, 1278–1288. [CrossRef]
16. Haque, A.; Bhuiya, A. The Role of Synthetic Inertia and Effective Load Modelling in Providing System Stability as Renewable Energy Penetration Increases. In Proceedings of the 2020 IEEE Industry Applications Society Annual Meeting, Detroit, MI, USA, 10–16 October 2020; pp. 1–6.
17. Jain, H.; Mather, B.; Jain, A.K.; Baldwin, S.F. Grid-Supportive Loads—A New Approach to Increasing Renewable Energy in Power Systems. *IEEE Trans. Smart Grid* **2022**, *13*, 2959–2972. [CrossRef]
18. Said, H.A.; García-Violini, D.; Faedo, N.; Ringwood, J.V. On the Ratio of Reactive to Active Power in Wave Energy Converter Control. *IEEE Open J. Control Syst.* **2024**, *3*, 14–31. [CrossRef]
19. Benavides, D.; Arévalo, P.; Criollo, A.; Tostado-Véliz, M.; Jurado, F. Multi-mode monitoring and energy management for photovoltaic-storage systems. *Renew. Energy* **2024**, *230*, 120820. [CrossRef]
20. Anjaiah, K.; Dash, P.K.; Bisoi, R.; Dhar, S.; Mishra, S.P. A new approach for active and reactive power management in renewable based hybrid microgrid considering storage devices. *Appl. Energy* **2024**, *367*, 123429. [CrossRef]
21. Arévalo, P.; Benavides, D.; Tostado-Véliz, M.; Aguado, J.A.; Jurado, F. Smart monitoring method for photovoltaic systems and failure control based on power smoothing techniques. *Renew. Energy* **2023**, *205*, 366–383. [CrossRef]
22. Liu, A.; Li, X.; Li, Y.; Hao, S.; Miao, Y.; Zheng, Y.; Xie, J.; Yao, Q. Collaborative scheduling method of active-reactive power for rural distribution systems with a high proportion of renewable energy. *Front. Energy Res.* **2024**, *12*, 1410694. [CrossRef]
23. Benbouhenni, H.; Bizon, N.; Colak, I.; Mosaad, M.I.; Yessef, M. Direct active and reactive powers control of double-powered asynchronous generators in multi-rotor wind power systems using modified synergetic control. *Energy Rep.* **2023**, *10*, 4286–4301. [CrossRef]
24. Fotopoulou, M.; Rakopoulos, D.; Petridis, S.; Drosatos, P. Assessment of smart grid operation under emergency situations. *Energy* **2024**, *287*, 129661. [CrossRef]
25. Li, Z.; Liu, F. Frequency and voltage regulation control strategy of Wind Turbine based on supercapacitors under power grid fault. *Energy Rep.* **2023**, *10*, 2612–2622. [CrossRef]
26. Calle-Prado, A.; Alepuz, S.; Bordonau, J.; Nicolas-Apruzzese, J.; Cortés, P.; Rodriguez, J. Model Predictive Current Control of Grid-Connected Neutral-Point-Clamped Converters to Meet Low-Voltage Ride-Through Requirements. *IEEE Trans. Ind. Electron.* **2015**, *62*, 1503–1514. [CrossRef]

27. Lyu, X.; Jia, Y.; Liu, T.; He, Y. Concurrent Optimal Re/Active Power Control for Wind Farms Under Low-Voltage-Ride-Through Operation. *IEEE Trans. Power Syst.* **2020**, *35*, 4956–4959. [CrossRef]
28. Wu, L.; Zhao, W.; Xu, M.; Xu, P.; Li, F.; Yang, Y.; Pan, Y. Mechanism Analysis and Suppression of Repeated Voltage Fluctuation Considering Fault Ride Through Characteristics of the Wind Turbine. *J. Glob. Energy Interconnect.* **2022**, *5*, 290–297.